Journal of Sound and Vibration (1999) **226**(3), 469–492
Article No. jsvi.1999.2264, available online at http://www.idealibrary.com on IDEAL®

BIFURCATION AND CHAOS IN GEARED ROTOR BEARING SYSTEM BY INCREMENTAL HARMONIC BALANCE METHOD

A. RAGHOTHAMA AND S. NARAYANAN

Machine Dynamics Laboratory, Department of Applied Mechanics, Indian Institute of Technology, Madras, Chennai, 600036, *India*

(*Received* 11 *August* 1998, *and in final form* 18 *March* 1999)

The periodic motions of a non-linear geared rotor-bearing system are investigated by the incremental harmonic balance (IHB) method. A path following procedure using arc length continuation technique is used to trace the bifurcation diagrams. The system exhibits a period doubling route and a quasiperiodic route to chaos in different regions of excitation frequency. The chaotic motions are investi gated by numerical integration and the Lyapunov exponents are computed. The periodic solutions and subharmonic solutions obtained by the IHB method compare very well with those obtained by numerical integration.

1. INTRODUCTION

In geared rotor-bearing systems, while modelling the dynamic behavior, non-linearities are induced due to gear backlash and bearing clearance. Backlash in the gear pair and clearances in the shaft-bearing system may be introduced to provide better lubrication and eliminate interference. These may also be induced due to manufacturing errors and wear. Backlash-induced torsional vibrations may cause tooth separation and impacts in geared rotor-bearing systems. Such impacts result in intense vibration and will cause noise problems and large dynamic loads, which may affect the life and reliability of geared drives. Thus, the analysis of geared rotor-bearing systems with non-linearities becomes important.

Non-linear dynamics of geared rotor-bearing system with multiple clearance was studied by Kahraman and Singh [1]. A three-degree-of-freedom (d.o.f.) model was developed which included non-linearities associated with radial clearances in the radial rolling element bearings and backlash between a spur gear pair. Several key issues such as non-linear modal interactions and differences between internal static transmission error excitation and external torque excitation were discussed. Parametric studies were presented and period doubling and quasiperiodic routes to chaos have been identified. Kahraman and Singh [2] have studied the frequency response characteristics of a non-linear geared rotor-bearing system with time-varying mesh stiffness. A single-degree-of-freedom (s.d.o.f.) spur gear model

0022–460X/99/380469 + 24 $30.00/0

with backlash and sinusoidal/periodic mesh stiffness, and a three d.o.f. model with clearance non-linearities associated with gear backlash and rolling element bearing with time-varying mesh stiffness were developed. The governing equations were solved by numerical integration. A strong interaction between time-varying stiffness and gear backlash was found, while the coupling between time-varying mesh stiffness and bearing clearance was found to be weak. The analytical results were found to be in good agreement with benchmark experimental results.

The s.d.o.f. spur gear model and three-d.o.f. model of a geared rotor bearing without time-varying mesh stiffness were analyzed for their dynamic behavior by the IHB method by Raghothama [3]. The periodic, subharmonic and period-doubling bifurcations were obtained by the IHB method and the results were shown to be in good agreement with numerically integrated results. A mechanical system with combined parametric excitation and clearance non-linearity was examined analytically and experimentally by Blankenship and Kahraman [4]. A generalized methodology was proposed based on the harmonic balance method. The mechanical system analyzed in their study has a significant relevance in automotive, aerospace, marine and industrial power transmission and gearing applications. The steady state forced response of a system with clearance subject to commensurate parametric and external forcing was investigated analytically by considering a mechanical oscillator with time-varying stiffness and a dead zone type clearance non-linearity by Kahraman and Blankenship [5]. A generalized multiple-term harmonic balance procedure is utilized to find periodic solutions. Interactions between periodically time-varying stiffness and forcing functions were characterized in the primary regimes. Closed-form impact criteria were derived for period 1 solutions. The effects of system parameters on subharmonic resonances were examined and experimental results were included which conclusively demonstrated the existence of subharmonic resonances in the geared systems. The importance of mean load effect has been highlighted in the study of whirling asymmetric shafts, where significant changes in system responses and stability occur under the influence of gravity by Padmanabhan and Singh [6]. They have studied the specific effect of mean load on the dynamic behavior of a Hill's oscillator with a clearance-type non-linearity and subjected to a periodic base displacement excitation. The parametric continuation technique and method of harmonic balance has been used for the analysis. Issues such as coupling between the mean load and dynamic response amplitude, and interaction between the parametric excitation and clearance non-linearity have been analysed.

The experimental results on a non-linear system with clearance subjected to combined parametric and external excitation were presented in a recent paper by Kahraman and Blankenship [7]. The experimental results showed subharmonic motions, jump phenomena, long periodic motions up to the order of period 9 and chaotic motions.

Wong *et al.* [8] have investigated a s.d.o.f. non-linear system subjected to harmonic excitation with un-symmetrical piecewise linear stiffness by the extended incremental harmonic balance method. Subharmonic, harmonic and superharmonic resonances and bifurcations were observed for the oscillator model

considered. The IHB method was extended by Lau and Zhang [9] to analyze periodic motions of systems with piecewise linear stiffness characteristics.

In this paper, the IHB method is used to obtain the periodic motions of a 3-d.o.f. non-linear model of a geared rotor system subjected to parametric and external harmonic excitations. The stability of the periodic motions is investigated by the Floquet theory and in combination with a path following and arc length parametric continuation procedure, the bifurcation behavior is traced. In the geared rotor-bearing system the non-linearities are induced by gear backlash and bearing clearances. The gear mesh stiffness is not only non-linear but time dependent also. The time-varying mesh stiffness arises due to change in the number of conjugate tooth pairs in contact during the involute action. This leads to the parametric excitation and the external excitation is caused by the static transmission error induced by kinematic errors and tooth deflections. The Jacobian matrix and the residue vector arising in the IHB formulations are derived explicitly. In addition to the familiar period doubling bifurcation scenario leading to chaos, in this example, a quasiperiodic route to chaos is also observed which occurs through an initial Hopf bifurcation. The periodic, subharmonic solutions and the bifurcation points obtained by the IHB method compare very well with the results obtained by numerical integration.

2. NON-LINEAR MODEL OF A GEARED ROTOR-BEARING SYSTEM

The geared rotor-bearing model considered in this study is shown in Figure 1(a). The model is essentially the same as considered by Kahraman and Singh [2]. The same model was also considered by numerical integration and the IHB method by the first author [3] for the system without parametric excitation. In this model, friction forces at the mesh point are assumed to be negligible. Because of this the transverse vibrations along the directions of pressure line and the vibrations along the direction perpendicular to the pressure line are uncoupled. Bearings and shafts that support the gears are represented by equivalent damping and non-linear stiffness elements as shown in Figure 1. The damping elements are characterized by linear viscous damping coefficients c_1 and c_2, and the non-linear stiffness elements are defined by non-linear force–displacement functions f_1 and f_2 with corresponding scaling constants k_1 and k_2. The effect of the prime mover and the load inertias are not considered. Also it is assumed that the system is symmetric about the plane of the gears and that the axial motion parallel to the shafts is negligible. A high-frequency internal excitation arising out of static transmission error is included in the equations of motion. External radial preloads F_1 and F_2 are also applied to both the rolling element bearings.

Under these assumptions, the equations of coupled transverse–torsional motion of the non-linear geared rotor-bearing system with time-varying mesh stiffness can be expressed as

$$m_1\ddot{y}_1 + c_1\dot{y}_1 + c_h(\dot{x} + \dot{y}_1 - \dot{y}_2 - \dot{e}) + k_1 f_1(y_1) + k_h(t) f_h(x + y_1 - y_2 - e(t)) = -F_1, \tag{1}$$

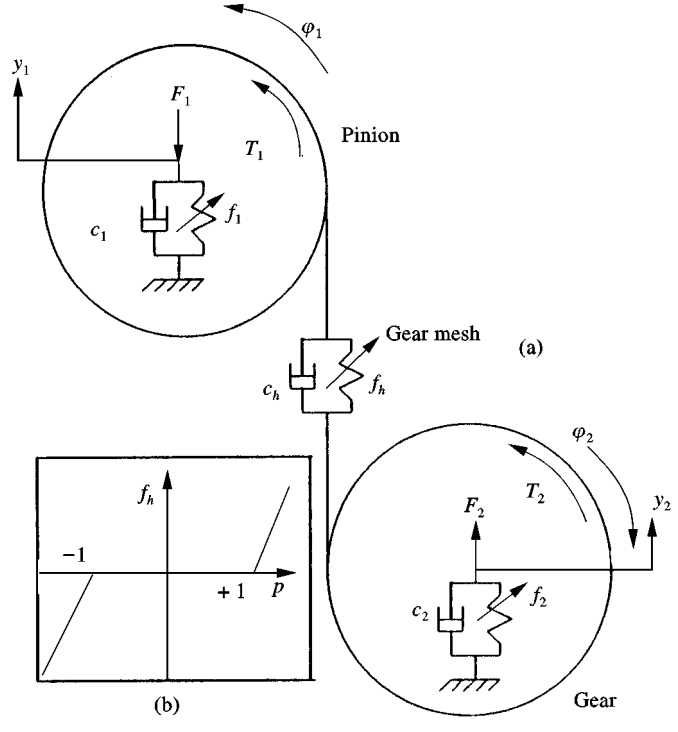

Figure 1. Non-linear model of a geared rotor-bearing system.

$$m_2\ddot{y}_2 + c_2\dot{y}_2 - c_h(\dot{x} + \dot{y}_1 - \dot{y}_2 - \dot{e}) + k_2 f_2(y_2) - k_h(t) f_h(x + y_1 - y_2 - e(t)) = F_2, \tag{2}$$

$$m\ddot{x} + c_h(\dot{x} + \dot{y}_1 - \dot{y}_2 - \dot{e}) + k_h(t) f_h(x + y_1 - y_2 - e) = F_m, \tag{3}$$

where

$$x(t) = \frac{d_1}{2}\varphi_1(t) - \frac{d_2}{2}\varphi_2(t), \quad m = \frac{1}{d_1^2/4I_1 + d_2^2/4I_2}, \quad F_m = \frac{2T_1}{d_1} = \frac{2T_2}{d_2},$$

$$k_h(t) = k_h(t + 2\pi/\omega) = k_{h0} + \sum_{r=1}^{\infty} k_{hr}\cos(r\omega t + \Phi_{hr}).$$

In these equations, the number of overdots represents the order of differentiation with respect to time t, y_i and φ_i are the transverse and torsional displacements of the ith gear ($i = 1, 2$), m is the equivalent gear pair mass, F_m is the average force transmitted through the gear mesh. m_1 and m_2 are the gear masses, I_1 and I_2 are the mass moments of inertia of the gears and d_1 and d_2 are the base circle diameters of

the gears. f_h is the non-linear function representing the force–displacement relation of the gear mesh. The time-varying mesh stiffness $k_h(t)$ is periodic and is expanded in Fourier series form with $k_{h0}(t)$ being the mean component and k_{hr} the harmonic components corresponding to integral multiples of the gear meshing frequency ω, which is also the fundamental excitation frequency corresponding to the internal displacement or static transmission error. c_h represents the linear viscous damping of the gear mesh and T_1 and T_2 are the input and output torque's at gears 1 and 2 and $e(t)$ is the static transmission error. The above equations are simplified further by defining a new variable $q(t)$, which is the difference between the dynamic transmission error and the static transmission error $e(t)$, that is

$$q(t) = x(t) + y_1(t) - y_2(t) - e(t). \tag{4}$$

In terms of $q(t)$, equations (1)–(3) become

$$\begin{bmatrix} m_1 & 0 & 0 \\ 0 & m_2 & 0 \\ -m & m & m \end{bmatrix} \begin{Bmatrix} \ddot{y}_1(t) \\ \ddot{y}_2(t) \\ \ddot{q}(t) \end{Bmatrix} + \begin{bmatrix} c_1 & 0 & c_h \\ 0 & c_2 & -c_h \\ 0 & 0 & c_h \end{bmatrix} \begin{Bmatrix} \dot{y}_1(t) \\ \dot{y}_2(t) \\ \dot{q}(t) \end{Bmatrix}$$
$$+ \begin{bmatrix} k_{11} & 0 & k_h(t) \\ 0 & k_{22} & -k_h(t) \\ 0 & 0 & k_h(t) \end{bmatrix} \begin{Bmatrix} f_1(y_1) \\ f_2(y_2) \\ f_h(q) \end{Bmatrix} = \begin{Bmatrix} -F_1 \\ F_2 \\ F_m - m\ddot{e}(t) \end{Bmatrix}. \tag{5}$$

A non-dimensional form of the above equations is obtained by letting

$$x_i(t) = y_i(t)/b_c, \quad p(t) = q(t)/b_c, \quad \omega_n = \sqrt{k_h/m}, \quad \omega_i = \sqrt{k_i/m_i}\,(i = 1, 2) \text{ and } \tau = \omega_n t,$$

where b_c is the characteristic length. The static transmission error $e(t)$ is considered as harmonic with $e(t) = e_0 \sin(\omega_h t)$ where ω_h is the fundamental frequency of the internal static transmission error excitation. Introducing the non-dimensional frequency $\Omega = \omega_h/\omega_n$, we get the following governing equations of motion in the non-dimensional form with time-varying mesh stiffness,

$$\begin{bmatrix} 1 & 0 & 0 \\ 0 & 1 & 0 \\ -1 & 1 & 1 \end{bmatrix} \begin{Bmatrix} \ddot{x}_1(\tau) \\ \ddot{x}_2(\tau) \\ \ddot{p}(\tau) \end{Bmatrix} + 2 \begin{bmatrix} \zeta_{11} & 0 & \zeta_{13} \\ 0 & \zeta_{22} & -\zeta_{23} \\ 0 & 0 & \zeta_{33} \end{bmatrix} \begin{Bmatrix} \dot{x}_1(\tau) \\ \dot{x}_2(\tau) \\ \dot{p}(\tau) \end{Bmatrix}$$
$$+ \begin{bmatrix} k_{11} & 0 & k_{13}(t) \\ 0 & k_{22} & -k_{23}(t) \\ 0 & 0 & k_{33}(t) \end{bmatrix} \begin{Bmatrix} f_1(x_1) \\ f_2(x_2) \\ f_h(p) \end{Bmatrix} = \{G(\tau)\} \tag{6}$$

where

$$\{G(\tau)\} = \{G\}_m + \{G(\tau)\}_i = \begin{Bmatrix} -G_1 \\ G_2 \\ G_m \end{Bmatrix} + \begin{Bmatrix} 0 \\ 0 \\ G_a\Omega^2 \end{Bmatrix} \sin \Omega\tau, \tag{7}$$

with

$$\zeta_{ii} = c_i/2m_i\omega_n, \quad \zeta_{i3} = c_h/2m_i\omega_n \ (i = 1, 2) \text{ and } \zeta_{33} = c_h/2m\omega_n$$

$$k_{ii} = \omega_i^2/\omega_n^2, k_{i3}(t) = k_h(t)/m_i\omega_n^2, G_i = F_i/m_i b_c\omega_n^2, \quad i = 1, 2$$

$$k_{ii} = \omega_i^2/\omega_n^2, \quad k_{i3} = m/m_i, \quad G_i = F_i/m_i b_c\omega_n^2 \quad (i = 1, 2)$$

$$k_{33}(t) = k_h(t) \Big/ k_m = 1 + \sum_{r=1}^{\infty} \varepsilon_r \cos(r\Omega t + \phi_r).$$

By taking $r = 1$ and $\phi_r = \pi$, we get $k_{33}(t) = 1 - \varepsilon \cos \Omega\tau$.

Also $G_m = F_m/(mb_c\omega_n^2)$, $G_a = e_0/b_c$ in which G_i and G_m are the dimensionless components of the mean force vector G_m, and G_h pertains to the internal excitation $\{G(\tau)\}_i$ force vector. The displacement force relation at the bearings is taken as linear in the current study but the algorithm presented is more general and can be used to get the solution by including the bearing non-linearities together with gear mesh clearance. In the present analysis at the gear mesh displacement force relationship is taken as clearance-type dead space functions with backlash $2b_h$ which is piecewise linear and can be written as

$$f_h(p) = \begin{cases} p(\tau) - b_h/b_c, & p(\tau) > b_h/b_c, \\ 0 & -b_h/b_c \leqslant p(\tau) \leqslant b_h/b_c, \\ p(\tau) + b_h/b_c, & p(\tau) < -b_h/b_c. \end{cases} \tag{8}$$

The value of b_h/b_c in the present study is taken as unity. This function is shown in Figure 1(b).

3. IHB METHOD FOR MULTI-DEGREE-OF-FREEDOM SYSTEMS

Consider the set of non-linear ordinary differential equations (ODE) representing the non-linear dynamical system of the following general form:

$$\mathbf{f}(\ddot{\mathbf{x}}, \dot{\mathbf{x}}, \mathbf{x}, \mathbf{F}, \Omega, \theta) = \mathbf{0}. \tag{9}$$

In this vector equation, $\mathbf{x} = \mathbf{x}(\theta)$ is the response of the non-linear system, or in general, the dependent variable vector, $\mathbf{F}$ is the vector of amplitudes of external

harmonic excitations, Ω represents a set of non-dimensional frequencies of relevance (non-dimensionalized with respect to a reference frequence), θ is a non-dimensional time and the number of overdots represents the order of differentiation with respect to θ.

The first step in applying the IHB method in obtaining a periodic solution of equation (9) is to increment from some initial guess of the solution $\mathbf{x}_0$, $\mathbf{F}_0$, Ω_0, to the actual solution $\mathbf{x}^*$, $\mathbf{F}^*$, Ω^*. In other words, an increment in $\mathbf{x}$, $\mathbf{F}$, Ω is sought which when added to the initial state $\mathbf{x}_0$, $\mathbf{F}_0$, Ω_0, produces the desired solution to equation (9) in an iterative manner. Using Taylor series expansion we get

$$\begin{aligned}&\mathbf{f}(\mathbf{x}_0 + \Delta\mathbf{x}, \dot{\mathbf{x}}_0 + \Delta\dot{\mathbf{x}}, \ddot{\mathbf{x}}_0 + \Delta\ddot{\mathbf{x}}, \mathbf{F}_0 + \Delta\mathbf{F}, \Omega_0 + \Delta\Omega, \theta)\\ &\quad = \mathbf{f}_0 + \left.\frac{\partial\mathbf{f}}{\partial\mathbf{x}}\right|_0 \Delta\mathbf{x} + \left.\frac{\partial\mathbf{f}}{\partial\dot{\mathbf{x}}}\right|_0 \Delta\dot{\mathbf{x}} + \left.\frac{\partial\mathbf{f}}{\partial\ddot{\mathbf{x}}}\right|_0 \Delta\ddot{\mathbf{x}} + \left.\frac{\partial\mathbf{f}}{\partial\mathbf{F}}\right|_0 \Delta\mathbf{F} + \left.\frac{\partial\mathbf{f}}{\partial\Omega}\right|_0 \Delta\Omega\\ &\qquad + \text{higher order terms} = \mathbf{0},\end{aligned} \tag{10}$$

where $\partial\mathbf{f}/\partial\mathbf{x}$, etc., are the matrices of the first partial derivatives of $\mathbf{f}$ with respect to $\mathbf{x}$, etc.

Neglecting the higher-order terms yields the incremental equation

$$\mathbf{f}_0 + \left.\frac{\partial\mathbf{f}}{\partial\mathbf{x}}\right|_0 \Delta\mathbf{x} + \left.\frac{\partial\mathbf{f}}{\partial\dot{\mathbf{x}}}\right|_0 \Delta\dot{\mathbf{x}} + \left.\frac{\partial\mathbf{f}}{\partial\ddot{\mathbf{x}}}\right|_0 \Delta\ddot{\mathbf{x}} + \left.\frac{\partial\mathbf{f}}{\partial\mathbf{F}}\right|_0 \Delta\mathbf{F} + \left.\frac{\partial\mathbf{f}}{\partial\Omega}\right|_0 \Delta\Omega = 0 \tag{11}$$

Noting that the terms $\partial\mathbf{f}/\partial\mathbf{x}|_0$, $\partial\mathbf{f}/\partial\dot{\mathbf{x}}|_0$, $\partial\mathbf{f}/\partial\ddot{\mathbf{x}}|_0$, $\partial\mathbf{f}/\partial\mathbf{F}|_0$, $\partial\mathbf{f}/\partial\Omega|_0$ can in general be time varying, equation (11) represents a set of linear, second order, variable coefficient, ODEs. Also, as $\mathbf{x}_0$, $\mathbf{F}_0$, Ω_0 approach $\mathbf{x}^*$, $\mathbf{F}^*$, Ω^*, $\mathbf{f}_0$ approaches zero. As the intention is to obtain periodic solutions to equation (11), a periodic solution can be obtained by expanding $\mathbf{x}$ in a truncated finite Fourier series and applying the Galerkin's procedure. Thus assume

$$\mathbf{x}(\theta) = \sum_{n=0}^{N} \alpha_n(\mathbf{a}_n \cos n\theta + \mathbf{b}_n \sin n\theta) \tag{12}$$

where $\mathbf{a}_n$ and $\mathbf{b}_n$ ($n = 0, 1, 2, \ldots, N$) are the Fourier coefficients and

$$\alpha_n = \begin{cases} 1 & \text{for } n \neq 0, \\ \frac{1}{2} & \text{for } n = 0. \end{cases} \tag{13}$$

The increment $\Delta\mathbf{x}$ can also be expanded in a Fourier series of the form

$$\Delta\mathbf{x}(\theta) = \sum_{n=0}^{N} \alpha_n(\Delta\mathbf{a}_n \cos n\theta + \Delta\mathbf{b}_n \sin n\theta), \tag{14}$$

where N represents the number of harmonics considered in the solution. When equations (12) and (14) are substituted into equation (11), since they represent only approximate solutions, the right-hand side of equation (11) will not be zero, but will contain a time-varying error term $\varepsilon(\theta)$. The explicit form of $\varepsilon(\theta)$ is given by

$$\varepsilon(\theta) = \mathbf{f}_0 + \left.\frac{\partial \mathbf{f}}{\partial \mathbf{x}}\right|_0 \sum_{n=0}^{N} \alpha_n (\Delta \mathbf{a}_n \cos \mathbf{n}\theta + \Delta \mathbf{b}_n \sin n\theta)$$

$$+ \left.\frac{\partial \mathbf{f}}{\partial \dot{\mathbf{x}}}\right|_0 \sum_{n=0}^{N} (-\mathbf{n}\Delta \mathbf{a}_n \sin \mathbf{n}\theta + \mathbf{n}\Delta \mathbf{b}_n \cos n\theta)$$

$$+ \left.\frac{\partial \mathbf{f}}{\partial \dot{\mathbf{x}}}\right|_0 \sum_{n=1}^{N} (-\mathbf{n}^2 \Delta \mathbf{a}_n \cos \mathbf{n}\theta - \mathbf{n}^2 \Delta \mathbf{b}_n \sin \mathbf{n}\theta) + \left.\frac{\partial \mathbf{f}}{\partial \mathbf{F}}\right|_0 \Delta \mathbf{F} + \left.\frac{\partial \mathbf{f}}{\partial \Omega}\right|_0 \Delta\Omega \quad (15)$$

The Galerkin method requires that the increments $\Delta \mathbf{a}_n$, $\Delta \mathbf{b}_n$, $\Delta \mathbf{F}$, $\Delta\Omega$ be chosen so as to minimize $\varepsilon(\theta)$, by making $\varepsilon(\theta)$ orthogonal to each term in the expansion (12), that is,

$$\int_0^{2\pi} \varepsilon(\theta) \begin{Bmatrix} \cos n\theta \\ \sin n\theta \end{Bmatrix} \mathrm{d}\theta = 0, \quad n = 0, 1, 2, \ldots, N. \quad (16)$$

Equation (16) represents $2N + 1$ algebraic linear equations in Δa_n, Δb_n. This can be written in matrix form as

$$\mathbf{R} = \mathbf{C}\, \Delta \mathbf{a} + \mathbf{P}\, \Delta \mathbf{F} + \mathbf{Q}\, \Delta\Omega, \quad (17)$$

where

$$\mathbf{R} = \begin{Bmatrix} \mathbf{R}_n^c \\ \mathbf{R}_n^s \end{Bmatrix}, \qquad \mathbf{C} = \begin{bmatrix} \mathbf{C}_n^{cc} & \mathbf{C}_n^{cs} \\ \mathbf{C}_n^{sc} & \mathbf{C}_n^{ss} \end{bmatrix}, \quad (18)$$

$$\Delta \mathbf{a} = \begin{Bmatrix} \Delta \mathbf{a}^c \\ \Delta \mathbf{b}^s \end{Bmatrix}, \qquad \Delta \mathbf{F} = \begin{Bmatrix} \Delta \mathbf{F}^c \\ \Delta \mathbf{F}^s \end{Bmatrix}, \quad (19)$$

$$\mathbf{P} = \begin{Bmatrix} \mathbf{P}_n^c \\ \mathbf{P}_n^s \end{Bmatrix}, \qquad \mathbf{Q} = \begin{Bmatrix} \mathbf{Q}_n^c \\ \mathbf{Q}_n^s \end{Bmatrix}. \quad (20)$$

$\Delta \mathbf{F}$ represents the increment in the amplitude of exciting force vector and $\Delta\Omega$ the increment in the frequency of excitation. $\mathbf{C}$ refers to the Jacobian matrix. $\Delta \mathbf{a}^c$, $\Delta \mathbf{b}^s$ are increments in the Fourier coefficients of the assumed solution. $\mathbf{R}$ represents the residue vector. In general, $\mathbf{P}$ is the parametric gradient vector and $\mathbf{Q}$ is frequency gradient vector.

The superscripts c and s refer to the cosine and sine coefficient terms respectively. The convergence of the periodic solution is checked by evaluating the following error estimates ε_1 and ε_2:

$$\varepsilon_1 = \sqrt{(\mathbf{R}^{c^2} + \mathbf{R}^{s^2})}, \qquad \varepsilon_2 = \sqrt{(\Delta\mathbf{a}^{c^2} + \Delta\mathbf{b}^{s^2})}, \tag{21}$$

Error estimate ε_1 indicates the closeness of the Fourier transform and the actual Fourier contents while ε_2 represents the Euclidean norm of the Newton–Raphson increments obtained during iteration. The iteration should be continued till the error estimate becomes less than an acceptable limit. By having a sufficient number of Fourier coefficients and iterations, the periodic solution with the prescribed error tolerance can be obtained. The Jacobian matrix and the residue vector for the piecewise linear system with cosine parametric excitation occurring in equation (6) are derived below. Considering in general the piecewise linear restoring force with cosine parametric excitation of the form

$$h(x) = \begin{cases} (x-1)(1-\cos\tau) & x > 1, \\ 0 & -1 \leqslant x \leqslant 1, \\ (x+1)(1-\cos\tau), & x < -1, \end{cases} \tag{22}$$

the components of the residue vector and the Jacobian matrix corresponding to equation (6) are given by

$$R_i^c = a_0 \sum_{l=0}^{L} h[E_\lambda(\theta_{l+1}) - E_\lambda(\theta_l)] + \sum_{l=0}^{L}\sum_{k=1}^{N} [a_k(A_{\lambda,k}(\theta_{l+1}) - A_{\lambda,k}(\theta_l))$$

$$+ b_k(B_{\lambda,k}(\theta_{l+1}) - B_{\lambda,k}(\theta_l))] \mp \sum_{l=0}^{L} [E_\lambda(\theta_{l+1}) - E_\lambda(\theta_l)], \quad i = 0,$$

$$R_i^c = R_i^{c0} + R_i^{cc} + R_i^{cs}, \quad i = 1, 2, \ldots, N,$$

$$R_i^{c0} = (a_0 \mp 1) \sum_{l=0}^{L} h\,[A_{\lambda,i}(\theta_{l+1}) - A_{\lambda,i}(\theta_l)],$$

$$R_i^{cc} = \frac{1}{2} \sum_{l=0}^{L} h \sum_{k=1}^{N} a_k[A_{\lambda,k+i}(\theta_{l+1}) - A_{\lambda,k+i}(\theta_l)$$

$$+ A_{\lambda,|k-i|}(\theta_{l+1}) - A_{\lambda,|k-i|}(\theta_l),$$

$$R_i^{cs} = \frac{1}{2} \sum_{l=0}^{L} h \sum_{k=1}^{N} b_k[B_{\lambda,k+i}(\theta_{l+1}) - B_{\lambda,k+1}(\theta_l)$$

$$+ \operatorname{sgn}(k-i)(B_{\lambda,|k-i|}(\theta_{l+1}) - B_{\lambda,|k-i|}(\theta_l))],$$

$$R_i^s = R_i^{s0} + R_i^{sc} + R_i^{ss}, \quad i = 1, 2, \ldots, N,$$

$$R_i^{s0} = (a_0 \mp 1) \sum_{l=0}^{L} h\,[B_{\lambda,i}(\theta_{l+1}) - B_{\lambda,i}(\theta_l)],$$

$$R_i^{sc} = \frac{1}{2} \sum_{l=0}^{L} h \sum_{k=1}^{N} a_k [B_{\lambda,k+i}(\theta_{l+1}) - B_{\lambda,k+i}(\theta_l) + \operatorname{sgn}(i-k)(B_{\lambda,|k-i|}(\theta_{l+1}) - B_{\lambda,|k-i|}(\theta_l))],$$

$$R_i^{ss} = \frac{1}{2} \sum_{l=0}^{L} h \sum_{k=1}^{N} b_k [-A_{\lambda,k+i}(\theta_{l+1}) + A_{\lambda,k+i}(\theta_l) + A_{\lambda,|k-i|}(\theta_{l+1}) - A_{\lambda,|k-i|}(\theta_l), \tag{23}$$

$$C_{ij}^{cc} = \sum_{l=0}^{L} h\,[E_\lambda(\theta_{l+1}) - E_\lambda(\theta_l)], \quad i = 0,\ j = 0,$$

$$C_{ij}^{cc} = \sum_{l=0}^{L} h\,[A_{\lambda,j}(\theta_{l+1}) - A_{\lambda,j}(\theta_l)], \quad i = 0, \quad j = 0, 1, 2, \ldots, N.$$

$$C_{ij}^{cc} = \sum_{l=0}^{L} h\,[A_{\lambda,i}(\theta_{l+1}) - A_{\lambda,i}(\theta_l)], \quad i = 0, 1, 2, \ldots, N, \quad j = 0.$$

$$C_{ij}^{cc} = \frac{1}{2} \sum_{l=0}^{L} h[A_{\lambda,i+j}(\theta_{l+1}) - A_{\lambda,i+j}(\theta_l) + A_{\lambda,|i-j|}(\theta_{l+1}) - A_{\lambda,|i-j|}(\theta_l)], \quad i = 1, 2, \ldots, N, j = 1, 2, \ldots, N, \tag{24}$$

$$C_{ij}^{cs} = \sum_{l=0}^{L} h[B_{\lambda,j}(\theta_{l+1}) - B_{\lambda,j}(\theta_l)] \quad i = 0, j = 1, 2, \ldots, N,$$

$$C_{ij}^{cs} = \frac{1}{2} \sum_{l=0}^{L} h[B_{\lambda,i+j}(\theta_{l+1}) - B_{\lambda,i+j}(\theta_l) + \operatorname{sgn}(j-i)(B_{\lambda,|i-j|}(\theta_{l+1}) - B_{\lambda,|i-j|}(\theta_l)) \quad i = 1, 2, \ldots, N, j = 1, 2, \ldots, N, \tag{25}$$

$$C_{ij}^{sc} = C_{ji}^{cs}, \tag{26}$$

$$C_{ij}^{ss} = \frac{1}{2} \sum_{l=0}^{L} h[-A_{\lambda,i+j}(\theta_{l+1}) + A_{\lambda,i+j}(\theta_l) + A_{\lambda,|i-j|}(\theta_{l+1}) - A_{\lambda,|i-j|}(\theta_l)]. \tag{27}$$

In these expressions, $A_{\lambda,i}$, $B_{\lambda,i}$, etc., are the result of the integrals occurring in the IHB method and the expressions to evaluate these terms are given in Appendix A.

L represents the number zeroes of the equation $|x(\theta)| = 1$. Thus, the evaluation of the above integrals requires the knowledge of the zeroes of the equation $|x(\theta)| = 1$. In the computer program, this is achieved at each iteration through a procedure that uses the bisection and interpolation methods on the transcendental equation $|x(\theta)| = 1$. Considering a period 2π, where $\theta_0 = 0$ and $\theta_{M+1} = 2\pi$, let there be M zeroes of $|x(\theta)| = 1$ between θ_0 and θ_{M+1} which are denoted as $\theta_1, \theta_2, \ldots, \theta_M$ ($\theta_1 < \theta_2 < \theta_3 < \cdots < \theta_M$). Let $S_1, S_2, \ldots, S_M$ be the sign of $|x(\theta)| - 1$, respectively, in the intervals $[\theta_0 - \theta_1], [\theta_1 - \theta_2], \ldots, [\theta_M - \theta_{M+1}]$. Now the corresponding step function will be written as

$$h = \begin{cases} 1, & S_i \geqslant 0 \\ 0, & S_i < 0 \end{cases} \quad i = 1, 2, 3, \ldots, M + 1. \tag{28}$$

4. PATH FOLLOWING AND PARAMETRIC CONTINUATION

The IHB method can be used to obtain both the stable and unstable periodic solutions. The stability of the periodic solutions can be investigated by the Floquet theory. Stability analysis of the periodic solutions also enables one to obtain the bifurcation points. In the Floquet theory, the stability of the periodic solutions is investigated by perturbing the state variables about the steady state solutions. The transformation matrix or the monodromy matrix is obtained, which transforms the state vector at an instant time to another instant of time one period ahead. If the absolute values of the eigenvalues of the monodromy matrix are less than unity the periodic solution is stable. The way in which the eigenvalues leaves the unit circle determines the nature of the bifurcations. The monodromy matrix is determined using a procedure given by Friedmann *et al.* [10]. The IHB method with variable parameter is ideally suited to parametric continuation for obtaining the response diagrams of non-linear systems. After obtaining the solution for a particular value of the parameter, the solution for new parameter values slightly perturbed from the old value can be obtained by using the previous solution as an approximation. In this paper, the parametric continuation is performed by the arc length procedure given by Leung and Chui [11]. The main aim of the path following and parametric continuation is to effectively trace the bifurcation sequence as a system parameter is varied. Introducing path parameter γ, the augmenting equation corresponding to equation (9) for a general m.d.o.f. system can be written as

$$g(x) - \gamma = 0, \tag{29}$$

where $\mathbf{x} = [\{\bar{\mathbf{a}}\}^T, \mathbf{F}]^T$, $\bar{\mathbf{a}} = \{\{\mathbf{a}_1^T, \mathbf{a}_2^T, \ldots, \mathbf{a}_N^T\}^T\}$ and $\mathbf{a}_i = \{\mathbf{a}_{io}, \mathbf{a}_{i1}, \ldots, \mathbf{a}_{iN}, \mathbf{b}_{i1}, \ldots, \mathbf{b}_{in}\}^T$. A good choice of the function $\mathbf{g}(\mathbf{x})$ is $\mathbf{g}(\mathbf{x}) = \mathbf{x}^T\mathbf{x}$. Considering the increments in $\bar{\mathbf{a}}$, $\mathbf{F}$ and γ in equation (29), we get the incremental equation as

$$\sum_{j=1}^{N(2M+1)} \frac{\partial \mathbf{g}}{\partial \bar{\mathbf{a}}_j} \{\Delta \bar{\mathbf{a}}_j\} + \frac{\partial \mathbf{g}}{\partial \mathbf{F}} \Delta \mathbf{F} - \Delta\gamma + \mathbf{g}(\mathbf{x}) - \gamma = 0, \tag{30}$$

where $\bar{\mathbf{a}}_j$ is the jth element of $\bar{\mathbf{a}}$.

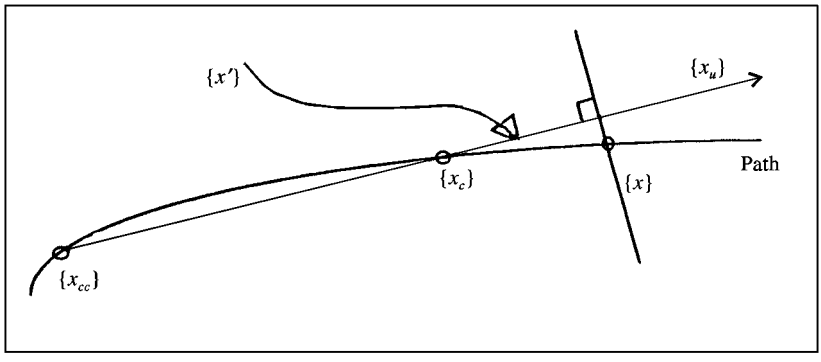

Figure 2. A portion of the equilibrium path.

Considering the portion of the equilibrium path of the solution branch shown in Figure 2, the augmenting equation (29) is written as

$$g(\mathbf{x}) - \gamma = \{\mathbf{x}'\}^T\{\mathbf{x} - \mathbf{x}_c\} = 0 \tag{31}$$

The first prediction of the new point $\mathbf{x}_u$ of the solution along the equilibrium path is given in terms of the two previous points $\mathbf{x}_c$ and $\mathbf{x}_{cc}$ as follows:

$$\mathbf{x}_u = \mathbf{x}_c + \Delta\gamma\mathbf{x}' \tag{32}$$

where

$$\mathbf{x}' = \{\mathbf{x}_c - \mathbf{x}_{cc}\}/\|\mathbf{x}_c - \mathbf{x}_{cc}\| \tag{33}$$

and $\Delta\gamma$ is an arbitrary step length taken in the computation by experience.

5. RESULTS AND DISCUSSION

5.1. PERIOD DOUBLING ROUTE TO CHAOS

The periodic motions of the geared rotor system given by equations (6) are obtained by the IHB method. The stability of the periodic solutions is investigated by the Floquet theory and the response diagrams are obtained by the path following technique and parametric continuation using the arc length procedure. The non-dimensional frequency Ω is taken as the bifurcation parameter in the same region of interest as studied in Kahraman and Singh [1] but with $\varepsilon = 0{\cdot}20$. While in their paper the main consideration is to obtain the response amplitude for a different set of parameters, in this paper we are mainly concerned with tracing the bifurcation diagrams and identifying the types of bifurcations:

$$G_m = 0{\cdot}1, \quad G_{ah} = 0{\cdot}05, \quad G_1 = G_2 = 0, \quad k_1/k_h = k_2/k_h = 5,$$

$$\zeta_{33} = 0{\cdot}05, \quad \zeta_{11} = \zeta_{22} = 0{\cdot}0$$

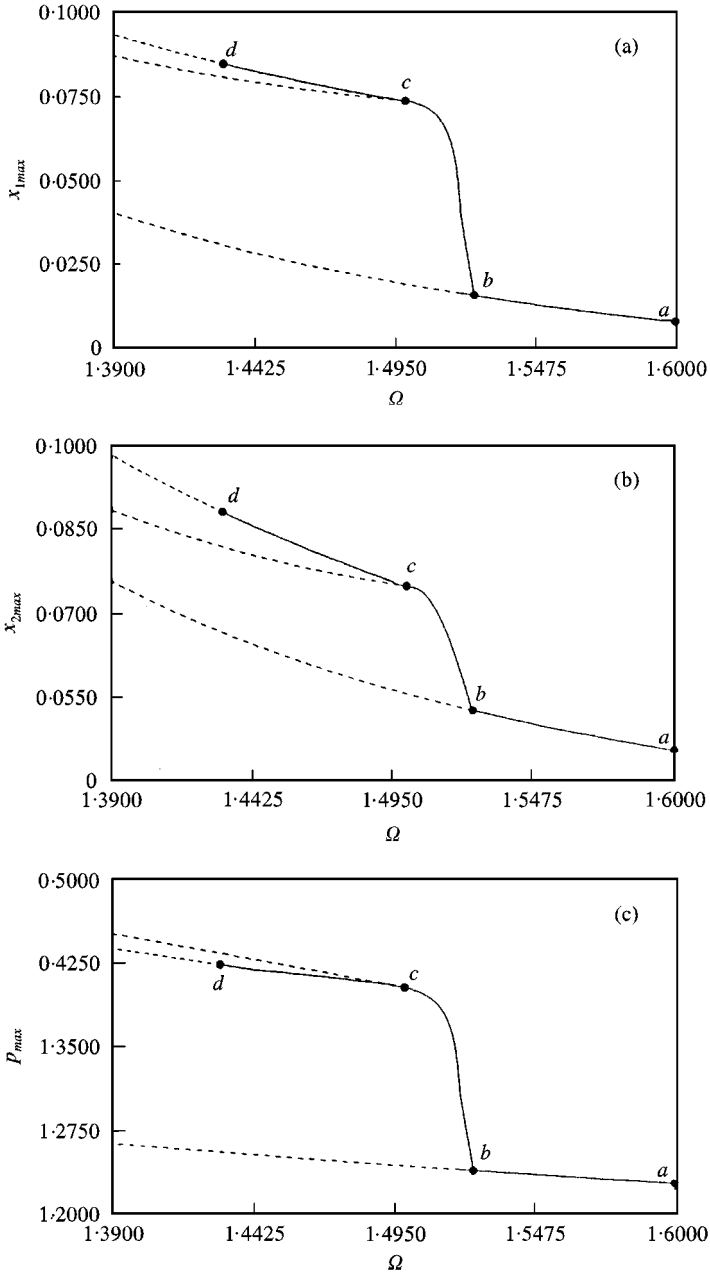

Figure 3. Response diagram in the period doubling region: (a) max x_1 versus Ω; (b) max x_2 versus Ω; (c) max p versus Ω.

$\zeta_{13} = \zeta_{23} = 0{\cdot}0125$, $\varepsilon = 0{\cdot}20$. Both the frequencies of parametric excitation and external excitation are taken as the same in the present study. The response diagrams are given in Figures 3(a–c). In these diagrams, starting from point "a", $\Omega = 1{\cdot}60$ and with the excitation frequency of the system decreasing, there exists

a period 1 response corresponding to the forcing period $2\pi/\Omega$ which bifurcates into a period 2 response at point "b", $\Omega = 1{\cdot}52$. The nature of bifurcation is period doubling and is confirmed by the movement of one of the Floquet multipliers corresponding to point "b", which leaves the unit circle in the -1 direction. For further decrease in the excitation frequency, the period 2 response undergoes further period doubling bifurcation resulting in a period 4 response at point "c", $\Omega = 1{\cdot}498$. The period 4 response bifurcates into a period 8 response at point "d", $\Omega = 1{\cdot}43$ for further decrease in the excitation frequency. One of the eigenvalues of the monodromy matrix moves out of the unit circle in the -1 direction corresponding to each of the period doubling bifurcations. In the response diagrams, the solid lines indicate stable responses and dashed lines indicate unstable responses.

The phase plane diagrams corresponding to the periodic and subharmonic responses obtained by the IHB method are given in Figures 4(a–l). The solid line indicates the response computed by the IHB method and the cross marks represent the solutions computed by numerical integration. The number of harmonics used in the finite Fourier series expansion in the IHB method are respectively 8, 16, 24, 32 for obtaining the period 1, 2, 4, and 8 responses. Excellent fit between the numerically integrated solutions and the IHB solution is thus observed. In obtaining the periodic solutions by the IHB method, the residue and norm of the increments of the Fourier coefficients are reduced to a value of less than $1{\cdot}0 \times 10^{-05}$.

The period doubling bifurcations lead ultimately to chaos. The chaotic trajectories are obtained by numerical integration. The time histories, phase plane diagrams, Poincare' sections and Fourier spectra corresponding to the chaotic response are presented in Figures 5a–l. In obtaining the Poincare' sections, the phase points are stroboscopically projected corresponding to one period of the excitation. The Poincare' sections have the appearance of a strange attractor typical of chaos. The Lyapunov exponents are computed by the Gram–Schmidt orthonormalization procedure given by Wolf *et al.* [12]. The Lyapunov exponents are shown in Figure 6. The largest Lyapunov exponent is positive in the chaotic region.

5.2. QUASIPERIODIC ROUTE TO CHAOS

There exists a quasiperiodic route to chaos in the lower ranges of the excitation frequency Ω. Again the non-dimensional frequency Ω is taken as the bifurcation parameter. The other parameter of the system are taken to be

$$G_2 = 0, \quad k_1/k_h = k_2/k_h = 1, \quad \zeta_{33} = 0{\cdot}05, \quad \zeta_{13} = \zeta_{23} = 0{\cdot}0125,$$

$$\zeta_{11} = \zeta_{22} = 0.01, \quad \varepsilon = 0{\cdot}2.$$

$G_m = 0{\cdot}1$, $G_{ah} = 0{\cdot}05$, $G_1 = 0$ in the quasiperiodic region. Both the frequencies of parametric excitation and external excitation are taken as the same as before. The

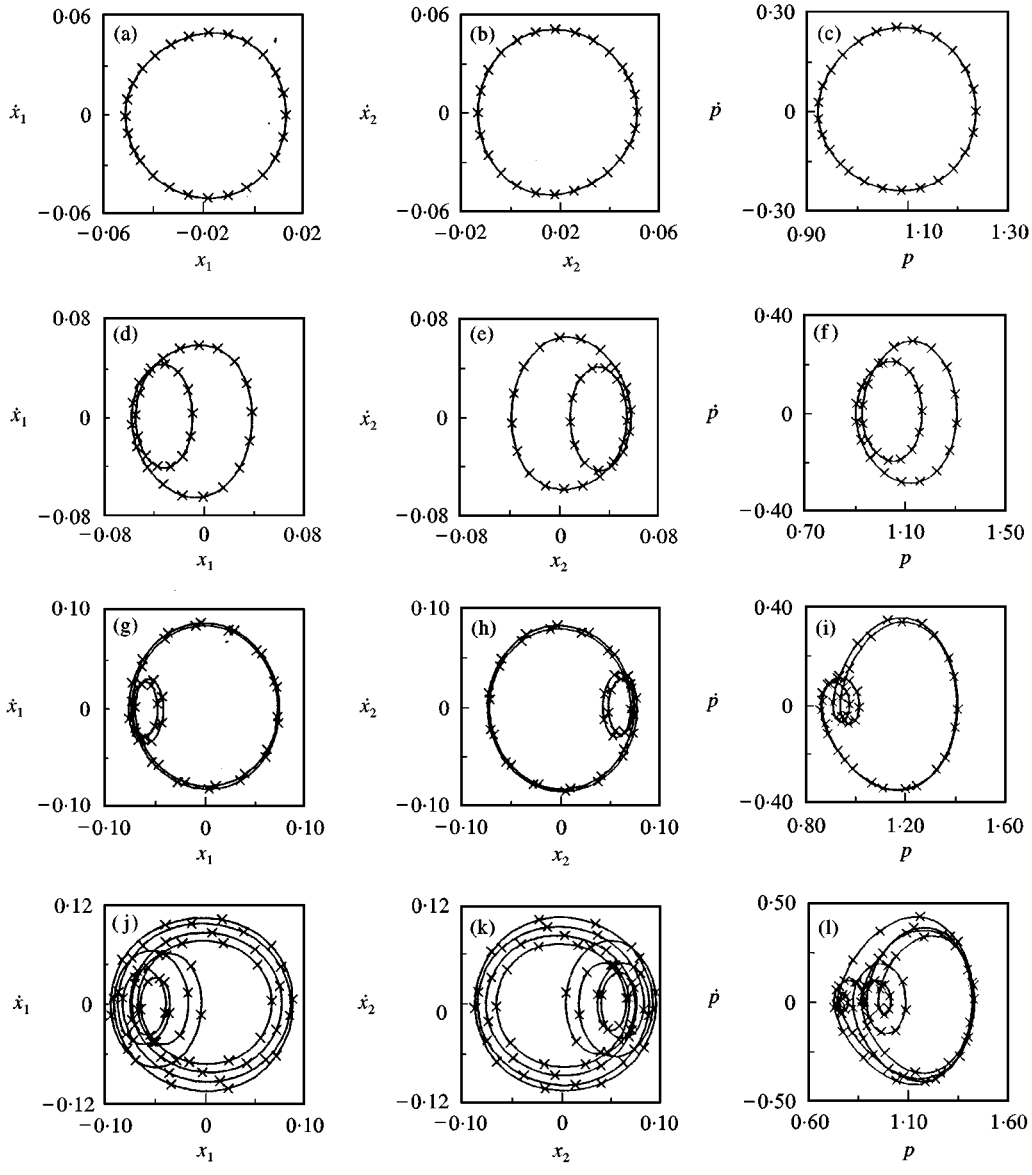

Figure 4. Phase planes for periodic and subharmonic motions (a–c) $\Omega = 1{\cdot}53$, period 1; (d–f) $\Omega = 1{\cdot}51$, period 2; (g–i) $\Omega = 1{\cdot}48$, period 4; (j–1) $\Omega = 1{\cdot}42$, period 8.

response diagrams for this case obtained by the IHB method with path following procedure are shown in Figures 7a–c. In these figures, starting form point "a", $\Omega = 0{\cdot}62$, there exists a period 1 response corresponding to the period of the external excitation $2\pi/\Omega$. This period 1 response continues to exist till point "b", $\Omega = 1{\cdot}06816$, at which a saddle-node bifurcation occurs evidenced by one of the eigenvalues of the monodromy matrix moving out of the unit circle along the $+1$ direction and the period 1 response becomes unstable. The response curve turns

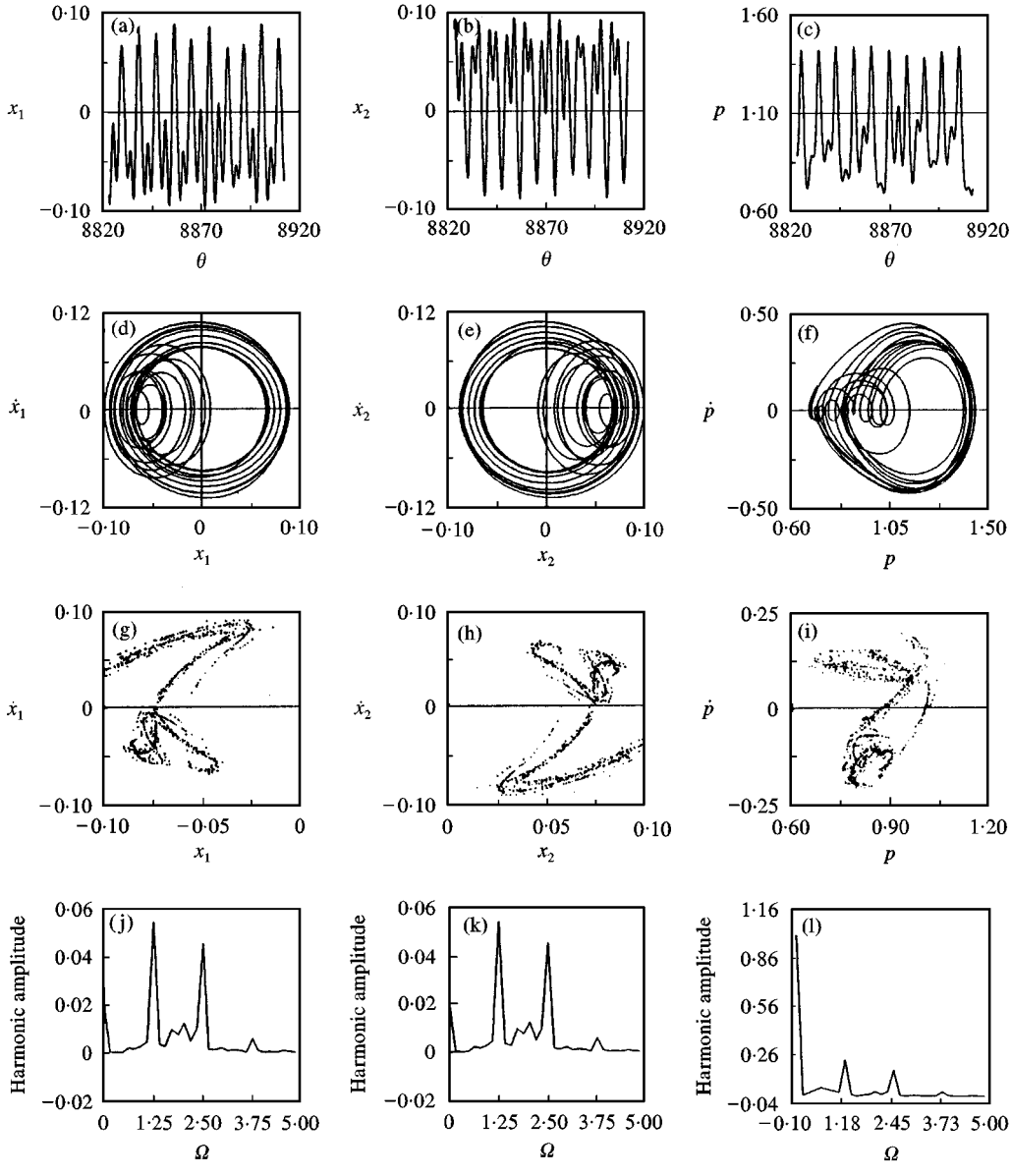

Figure 5. Chaotic motion in the period doubling region $\Omega = 1{\cdot}40$, (a–c) Time history, (d–f) phase plane; (g–i) Poincare' section; (j–l) Fourier spectrum.

back now for decreasing values of Ω, and at point "c", $\Omega = 0{\cdot}9591$ another saddle-node bifurcation takes place with one of the Floquet multipliers entering the unit circle from the $+1$ direction and the period 1 response becomes again stable. Thus, in between points "b" and "c" there are multiple period 1 responses, two stable period 1 responses and one unstable period 1 response. The phase planes of the two stable period 1 solutions and the one unstable period 1 solution obtained by the IHB method are given in Figures 8a–c at $\Omega = 0{\cdot}99$. The numerically

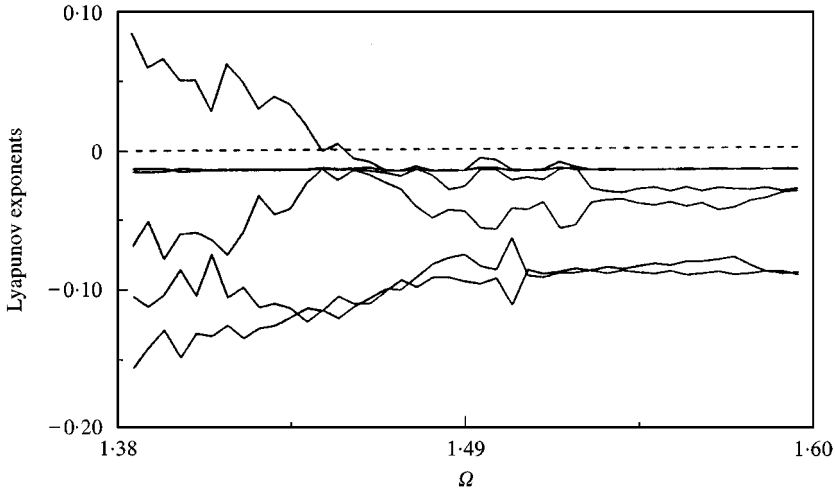

Figure 6. Lyapunov exponents in the period doubling region.

integrated solutions are superposed on the IHB solutions by the "x" mark showing the excellent match between the two with the increasing Ω corresponding to point "c", the period 1 response continues till point "d", $\Omega = 1{\cdot}3122$, at which it loses stability by a Hopf bifurcation resulting in a quasiperiodic response. This is evidenced by the movement of a pair of complex conjugate eigenvalues of the monodromy matrix moving radially out of the unit circle in the complex plane. The quasiperiodic response bifurcates into chaotic response in the region "d" to "e", $\Omega = 1{\cdot}5486$. At "e" the unstable period 1 response becomes again stable and a pair of complex conjugate eigenvalues of the monodromy matrix enters the unit circle radially. The time histories, phase plane diagrams, Poincare' sections and Fourier spectra of the period 1 response just before the Hopf bifurcation at point "d", $\Omega = 1{\cdot}25$, for the systems are given in Figures 9(a–l). The time histories, phase plane diagrams, Poincare' sections and Fourier spectra of the bifurcated quasiperiodic response at $\Omega = 1{\cdot}46$ for the system are shown in Figures 10(a–l). From the Fourier spectrum of the period 1 response shown in Figures 9(j–l), we can see that the spectrum shows an additional peak apart from the one corresponding to the excitation frequency, which is typical of torus 2 bifurcation which leads to the quasiperiodic motion. The Poincare' sections for this case are closed curves which are typical of a quasiperiodic response. The time histories, phase plane diagrams, Poincare' sections and Fourier transforms of the chaotic response at $\Omega = 1{\cdot}48$ are shown in Figures 11(a–l).

The Lyapunov exponents are also computed for these parameter values and the variation of the Lyapunov exponents with Ω as the parameter is shown in Figure 12. It can be observed that one of the Lyapunov exponents moves around the zero line in the region corresponding to the regions "d"–"e" representing the quasiperiodic region and crossing the zero axis on the positive side for a small region of chaotic behavior. The Lyapunov exponents for the chaotic trajectories at

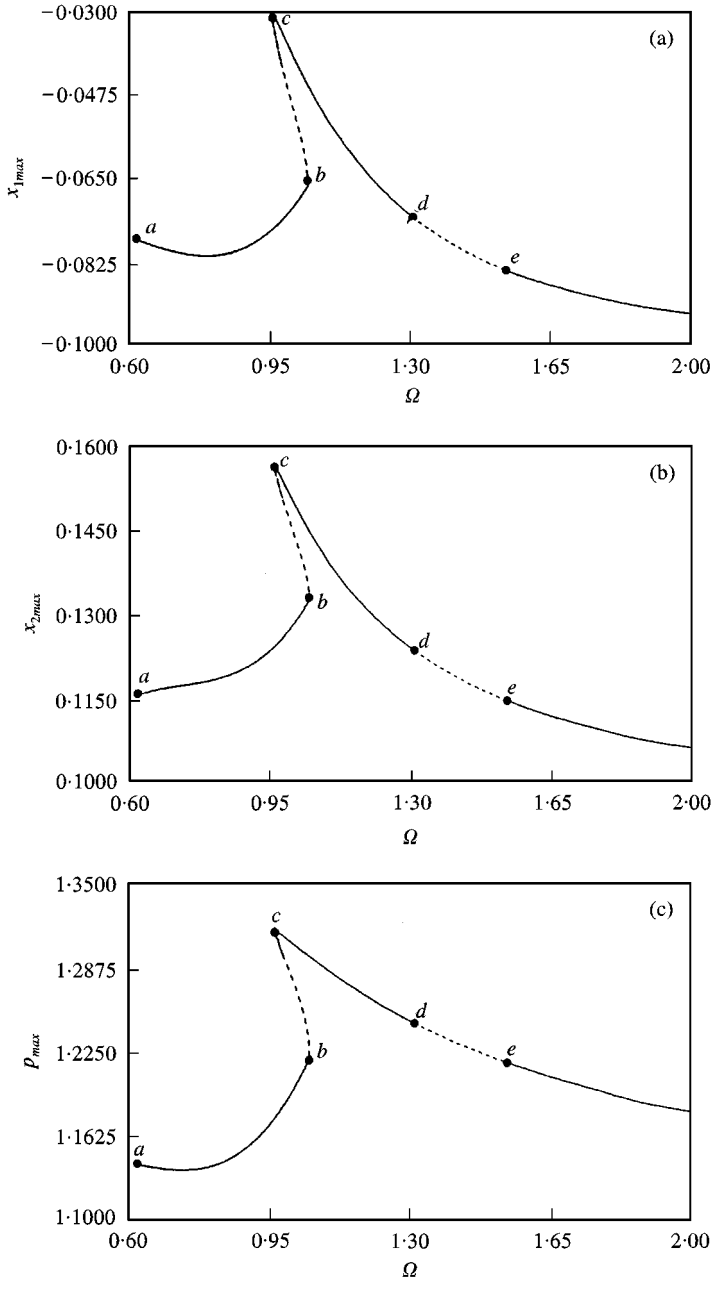

Figure 7. Response diagram in the quasiperiodic region: (a) max x_1 versus Ω, (b) max x_2 versus Ω; (c) max p versus Ω.

$\Omega = 1{\cdot}48$ for the system are 0·0124, −0·0130, −0·0157, −0·0365, −0·0595, −0·1616. Also in the parameter regions studied in this paper, similar types of response behavior have been shown by Kahraman and Singh [1] but without time-varying mesh stiffness.

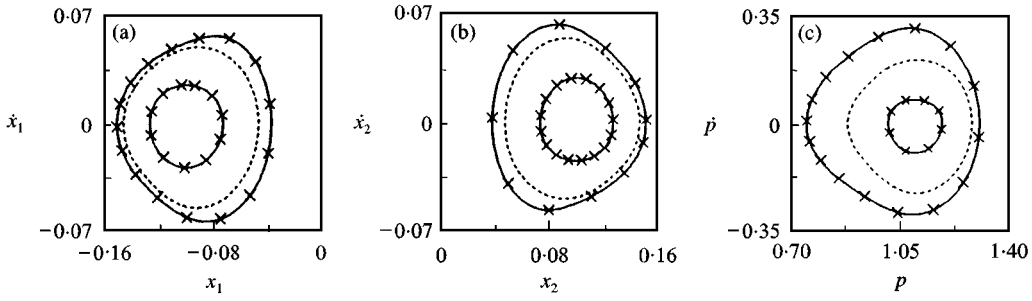

Figure 8. Multiple responses at $\Omega = 0{\cdot}99$.

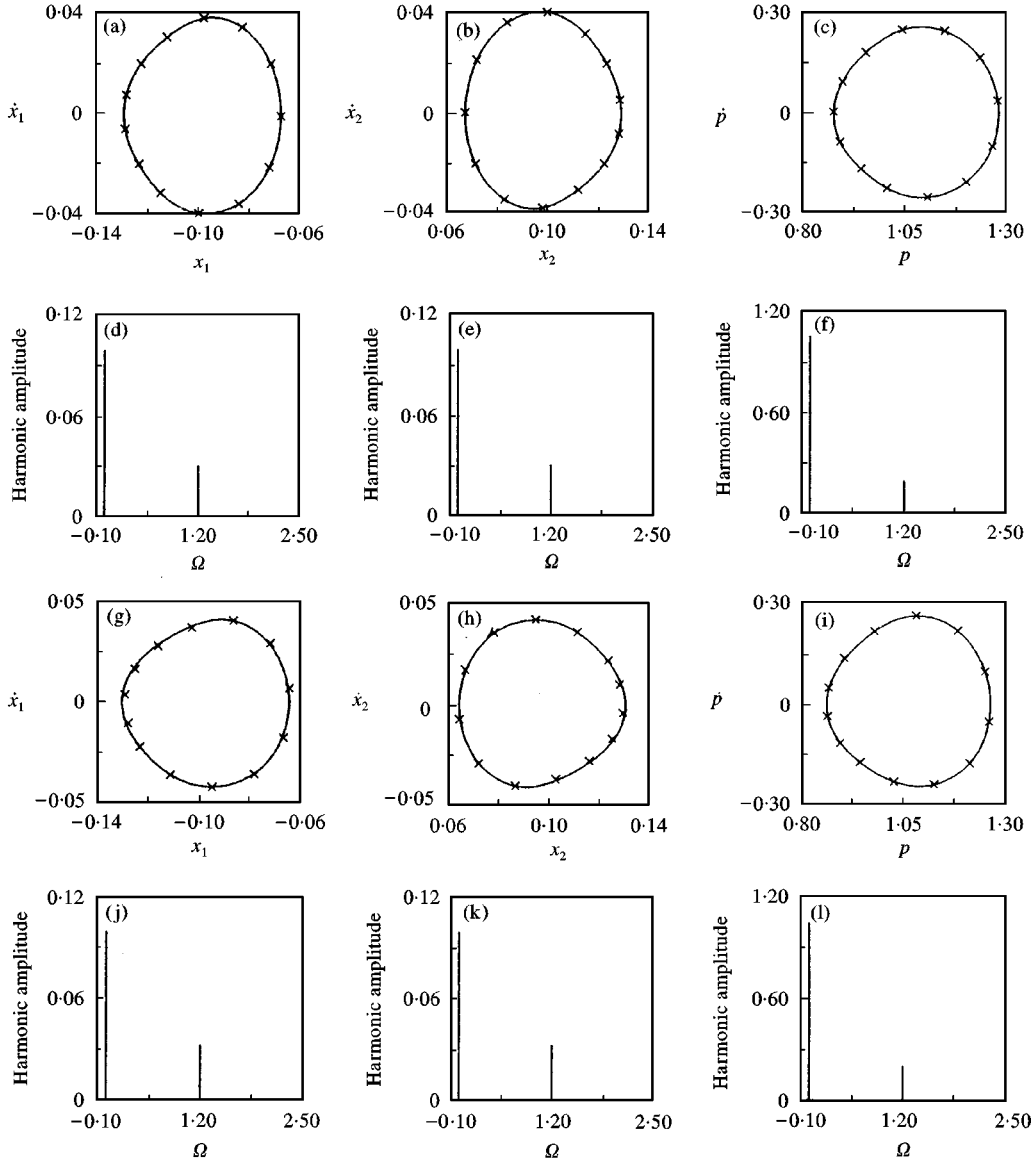

Figure 9. Phase planes and Fourier transform of the period 1 response at $\Omega = 1{\cdot}20$.

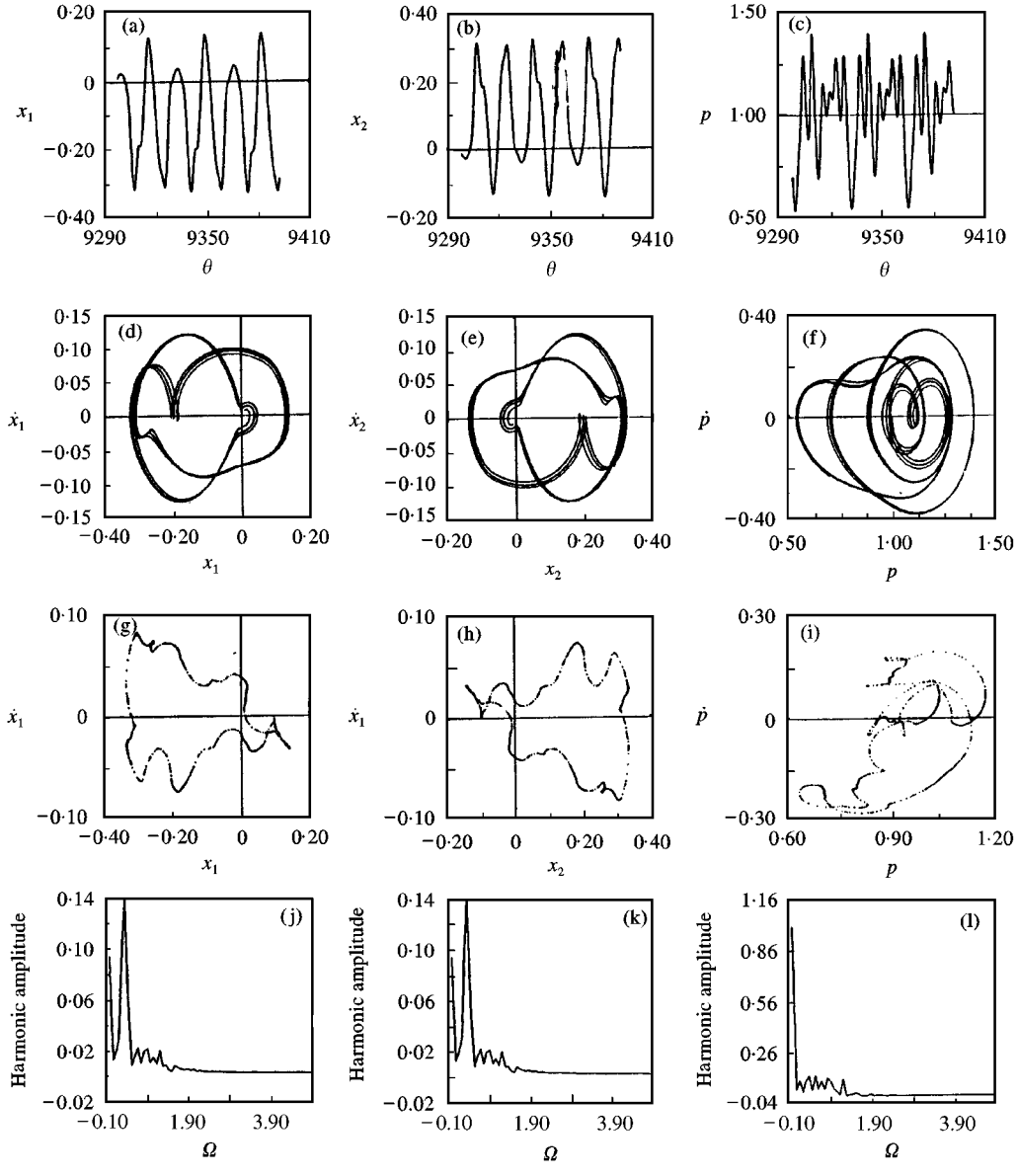

Figure 10. Quasiperiodic response $\Omega = 1{\cdot}46$. (a–c) Time history; (d–f) phase plane; (g–i) Poincare' section; (j–l) Fourier spectrum.

6. CONCLUSIONS

In this paper, the periodic motions of three d.o.f. geared rotor-bearing system with piecewise linear stiffness characteristics and subjected to parametric and external harmonic excitations are obtained by the IHB method. The elements of the Jacobian matrix and the residue vector occurring in the IHB formulations are

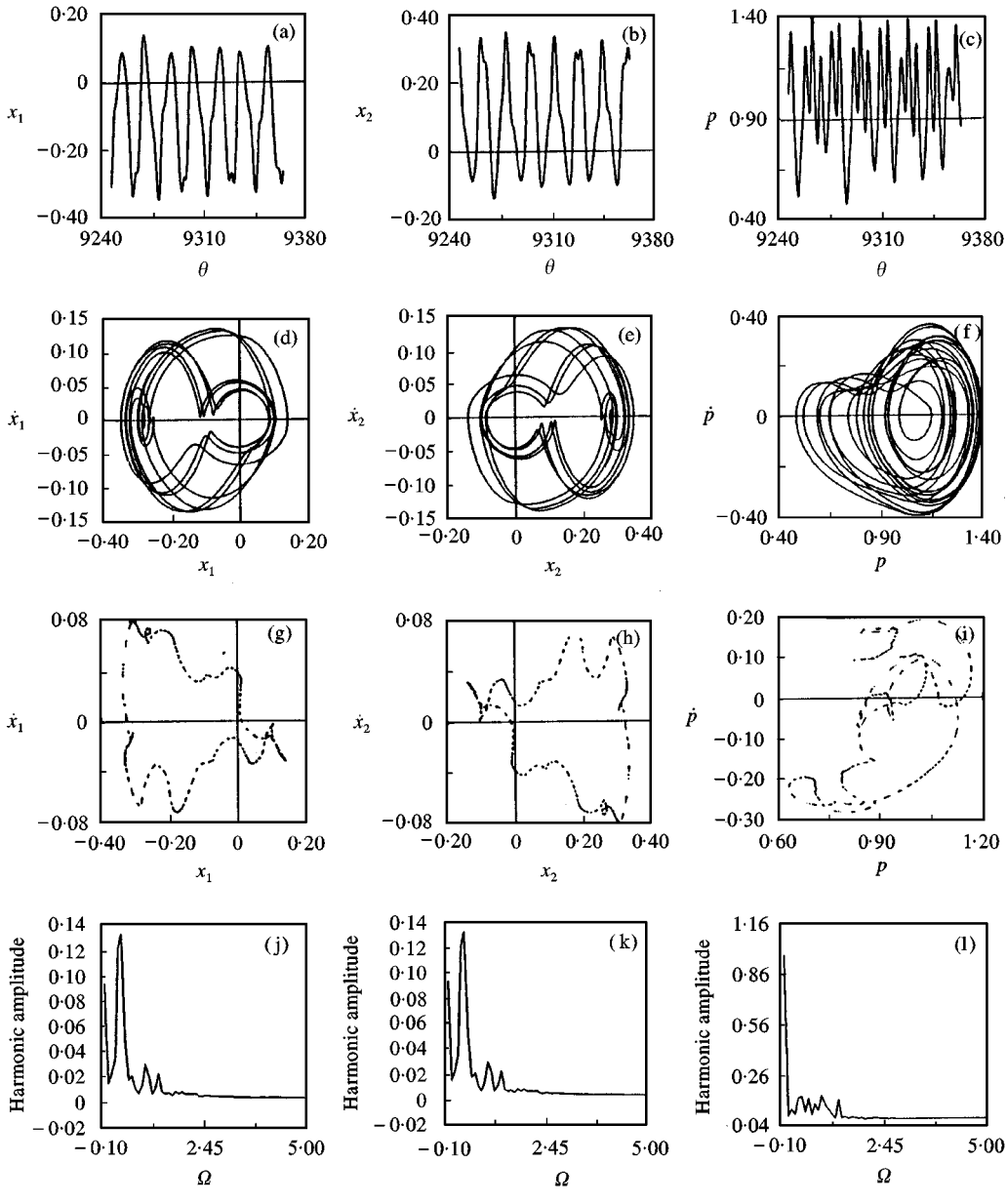

Figure 11. Chaotic response $\Omega = 1{\cdot}48$. (a–c) Time history; (d–f) phase plane; (g–i) Poincare' section; (j–l) Fourier spectrum.

explicitly derived. The periodic responses of the geared rotor-bearing system computed by the IHB method compare very well with the numerically obtained solutions. The bifurcation points and the response diagrams are obtained by combining the IHB method with the path following technique. The bifurcation points also match well with the numerically integrated results. A period doubling as

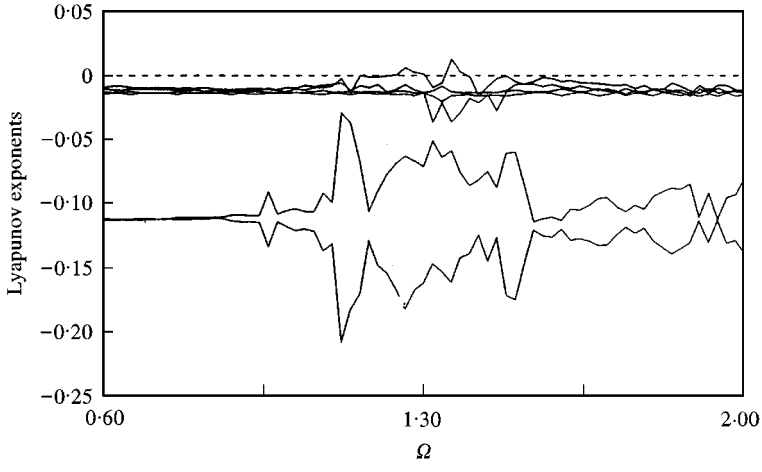

Figure 12. Lyapunov exponents in the quasiperiodic region.

well as a quasiperiodic route to chaos are observed in different ranges of excitation frequencies. Saddle-node bifurcations leading to multiple steady state solutions are also present. The example considered demonstrates the effectiveness of the IHB method in obtaining periodic solutions of m.d.o.f. systems with piecewise non-linearities.

REFERENCES

1. A. Kahraman and R. Singh 1991 *Journal of Sound and Vibrations* **144**, 469–506. Nonlinear dynamics of a geared rotor bearing system with multiple clearance.
2. A. Kahraman and R. Singh 1991 *Journal of Sound and Vibration* **146**, 135–156. Interactions between time-varying mesh stiffness and clearance nonlinearities in geared system.
3. A. Raghothama 1993 *M.S. thesis, Indian Institute of Technology, Madras.* Bifurcation and chaos in Gear and cam mechanisms with clearance type of nonlinearities.
4. G. W. Blankenship and A. Kahraman 1995 *Journal of Sound and Vibration* **185**, 743–765, Steady state forced response of a mechanical oscillator with combined parametric excitation and clearance type nonlinearity.
5. A. Kahraman and G. W. Blankenship 1996 *Journal of Sound and Vibration* **194**, 317–336. Interactions between commensurate parametric and forcing excitations in a system with clearance.
6. C. Padmanabhan and R. Singh 1996 *Journal of Acoustical Society of America* **99**, 324–334. Analysis of periodically forced nonlinear Hill's oscillator with application to a geared system.
7. A. Kahraman and G. W. Blankenship 1997 *Journal of Applied Mechanics* **64**, 217–226 Experiments on nonlinear dynamic behavior of an oscillator with clearance and periodically time-varying parameters.
8. C. W. Wong, W. S. Zhang and S. L. Lau 1991 *Journal of Sound and Vibration* **149**, 91–105. Periodic forced vibration of unsymmetrical piecewise linear systems by incremental harmonic balance method.
9. S. L. Lau and W.-S. Zhang 1992 *Journal of Applied Mechanics* **59**, 153–160. Nonlinear vibrations of piecewise linear systems by incremental harmonic balance method.

10. P. FRIEDMANN, C. E. HAMMOND and T. H. WOO 1977 *International Journal of Numerical Methods in Engineering* **11**, 1117–1136. Efficient numerical treatment of periodic systems with application to stability problems.
11. A. Y. T. LEUNG and S. K. CHUI 1995 *Journal of Sound and Vibration* **181**, 619–633. Nonlinear vibration of coupled Duffing oscillators by an improved incremental harmonic balance method.
12. A. WOLF, J. B. SWIFT, H. L. SWINNEY and J. A. VASTANO 1985 *Physica* **16D**, 285–331 Determining Lyapunov exponents from a time series.

APPENDIX A: TERMS APPEARING IN EQUATIONS (23)–(27) IN THE IHB FORMULATION

$$A_{m,n}(\theta_l) = \theta_l\left[\frac{\sin(m-n)\theta_l}{(m-n)\theta_l} + \frac{\sin(m+n)\theta_l}{(m+n)\theta_l}\right],$$

$$B_{m,n}(\theta_l) = \begin{cases} \theta_l\left[\dfrac{\cos(m-n)\theta_l}{(m-n)\theta_l} - \dfrac{\cos(m+n)\theta_l}{(m+n)\theta_l}\right] & \text{if } m \neq n, \\ -\theta_l\left[\dfrac{\cos(2m\theta_l)}{(2m\theta_l)}\right] & \text{if } m = n, \end{cases}$$

$$C_{m,n}(\theta_l) = B_{m,n}(\theta_l),$$

$$D_{m,n}(\theta_l) = \theta_l\left[\frac{\sin(m-n)\theta_l}{(m-n)\theta_l} - \frac{\sin(m+n)\theta_l}{(m+n)\theta_l}\right],$$

$$E_m(\theta_l) = \theta_l\left[\frac{\sin m\,\theta_l}{m\,\theta_l}\right],$$

$$F_m(\theta_l) = -\theta_l\left[\frac{\cos m\,\theta_l}{m\,\theta_l}\right].$$

APPENDIX B: LIST OF SYMBOLS

b	backlash
c	viscous damping coefficient
d	diameter
e	static transmission error
f	non-linear displacement function
F, G	force
I	rotary inertia
k	stiffness
m	mass
p	relative displacement
q	displacement
t	time

T	torque
x	relative displacement
y	transverse displacement
ϕ	phase angle
φ	an angle
k	dimensionless stiffness
ω	natural frequency
Ω	excitation frequency
ζ	damping ratio